Title
Prediction of far-field wind turbine noise propagation with parabolic equation

Journal
The Journal of the Acoustical Society of America, 140(2)

ISSN
0001-4966

Authors
Lee, Seongkyu
Lee, Dongjai
Honhoff, Saskia

Publication Date
2016-08-01

DOI
10.1121/1.4958996

Peer reviewed

Prediction of Far-Field Wind Turbine Noise Propagation with Parabolic Equation

Seongkyu Lee[a)]

Department of Mechanical and Aerospace Engineering

University of California, Davis

Davis, California 95616

and

Dongjai Lee and Saskia Honhoff

Renewable Engineering - Aero and Acoustics

General Electric Power & Water, Greenville, SC, 12309, USA

[a)]e-mail: skulee@ucdavis.edu

Sound propagation of wind farms is typically simulated by the use of engineering tools that are neglecting some atmospheric conditions and terrain effects. Wind and temperature profiles, however, can affect the propagation of sound and thus the perceived sound in the far field. A better understanding and application of those effects would allow a more optimized farm operation towards meeting noise regulations and optimizing energy yield. This paper presents the Parabolic Equation (PE) model development for accurate wind turbine noise propagation. The model is validated against analytic solutions for a uniform sound speed profile, benchmark problems for nonuniform sound speed profiles, and field sound test data for real environmental acoustics. It is shown that PE provides good agreement with the measured data, except upwind propagation cases in which turbulence scattering is important. Finally, the PE model uses computational fluid dynamics (CFD) results as input to accurately predict sound propagation for complex flows such as wake flows. It is demonstrated that wake flows significantly modify the sound propagation characteristics.

I. Introduction

For most wind farm projects, building permits are subject to compliance with local noise restrictions, i.e. maximum allowable sound pressure levels at farm boundaries or residential locations at typical distances from 600 - 2000 m. Accordingly, upfront simulations of the wind farm noise propagation into the far field is an inherent part of most wind farm developments. In highly populated areas and noise constrained regions, wind farms may need to run in curtailed operation with reduced energy yield in order to comply with the noise restrictions. The quality of the noise propagation simulation is thus an important factor for meeting the noise requirements and optimizing energy yield. Sound pressure levels in the far field of wind farms are typically modelled with simple engineering tools[15;19;22;26] that provide a quick assessment of noise contours. These models take into account a number of environmental factors such as atmospheric absorption, ground absorption and humidity. However, they usually cannot differentiate propagation effects for a wide range of wind and temperature profiles or complex terrain effects.

Over the past few years, physics-based noise propagation models have also been applied to predict far-field wind turbine noise in complex meteorological conditions or complex terrains. The two most prominent advanced models are the ray acoustics and parabolic equation (PE) model.

Prospathopoulos and Voutsinas[27;28] used the ray-tracing method to predict noise from isolated wind turbine and wind parks. The ray-tracing method is identifying the trajectory of eigenrays by solving the ray trajectory equations and then superposing the eigenray contributions arriving at the ground. They performed a detailed parameter sensitivity study including turbulence and wind direction effects. Heimann, et al.[12] used the ray-tracing method to investigate the effect of turbine wake flows on sound propagation. They showed that sound refraction associated with wake flows increases the sound pressure levels at large distances. Their study is not complete in a sense that the propagation distance was limited to around 1km and different wind shear effects were not considered.

In the PE method, the one-way Helmholtz equation is solved with spatially varying wavenumber or the speed of sound. The PE method has been widely used in underwater acoustics[7;17;21;31]. Gilbert and White[11] showed good comparisons between the PE method and measured data for neutral and downward refraction conditions in the atmosphere.

Cheng[6] formulated 3-D PE equations and tested different wind direction effects on sound propagation. Kaliski and Wilson[20] used the PE method for realistic speed of sound profiles to predict wind turbine noise and compared the PE results with engineering models. They established that for stable conditions, engineering models over-predict the noise level at far-field. Bolin and Boué[4] used the Green's Function PE (GFPE) method for off-shore wind turbine applications. They showed the impact of low level jets on long range sound propagation and presented good agreement between the prediction and data measured up to 10km away from the source. Johansson[18] applied the Crank-Nicholson PE (CNPE) method for off-shore wind turbine noise. The paper used a boss theory to describe the rough surface of ocean surface waves as a modification of the surface impedance. Low level jet and range-dependent wind profiles for the shoreline were used in the paper. The paper demonstrated that due to the refraction effects, the sound attenuation follows cylindrical spreading rather than spherical spreading. Mylonas[25] used the CNPE for sound propagation of wind turbines over water and they compared PE results with ISO9613-2, the Danish method and the Swedish method for sound propagation.

The current paper chooses the PE method for far-field wind turbine noise predictions. In general, the PE method is more accurate for complex wind and temperature profiles than the ray-tracing method. In addition, the ray-tracing method uses a high-frequency assumption so that it is not appropriate to predict the propagation of low-frequency noise that is important for wind turbine noise. One disadvantage of the PE method is that it requires a significant computation time for high frequency noise. The current paper limits the frequency range up to 1kHz since higher frequency than 1kHz makes little contribution to the overall sound pressure level at far-field due to large atmospheric absorption attenuation.

The goals of the current paper are to further validate the PE model against measured far-field noise data and to apply the PE model to realistic wind turbine noise propagation conditions. In particular, the PE method uses CFD results as input to simulate sound propagation under complex wind profiles and to investigate the detailed understanding of the wake flows on sound propagation. In section II, the theory and mathematical model of the PE method is described. In section III, the PE method is compared with analytic solutions, benchmark problems, and far-field sound measurement. In section IV, a CFD-based actuator disk model is used to provide mean shear flows that are used in the PE method as input to predict the sound propagation of wind turbine noise within wake flows. Finally, conclusions and suggestions for future work are discussed.

II. Numerical Methods

A. Parabolic Equation

The current paper uses the Crank-Nicholson PE (CNPE) method[11] to predict wind turbine noise propagation. To better understand the new application and implementation of the CNPE method into wind turbine noise propagation, brief mathematical formulations for the CNPE are reviewed in this section.

With the axisymmetric approximation, the three-dimensional Helmholtz equation becomes the two-dimensional Helmholtz equation:

$$\frac{\partial^2 q}{\partial r^2} + \frac{\partial^2 q}{\partial z^2} + k^2 q = 0 \tag{1}$$

where r denotes the propagation range variable, z the height variable, k the effective wavenumber. The quantity q is related to the complex pressure amplitude, p, which is given as

$$q = p\sqrt{r}. \tag{2}$$

This axisymmetric approximation is the approximation of far-field sound propagation.

Equation (1) can be reformulated into

$$[\partial_r - iH_1(z)][\partial_r + iH_1(z)]q = 0 \tag{3}$$

where $\partial_r \equiv \partial/\partial r$ and

$$H_1(z) = k_a\sqrt{1+s} \tag{4}$$

$$s = k_a^{-2}\delta k^2(z) + k_a^{-2}\partial_z^2 \tag{5}$$

$$\delta k^2(z) = k^2(z) - k_a^2 \tag{6}$$

If we are interested in one-way sound propagation from sources to receptors, Eq. (3) is reduced to the one-way propagation equation

$$[\partial_r - iH_1(z)]q = 0 \tag{7}$$

The approximation of the square-root operator Eq. (4) by

$$H_1(z) = k_a(1 + \frac{1}{2}s) \tag{8}$$

yields the narrow-angle PE

$$\partial_r\psi = \frac{1}{2}ik_a s\psi \tag{9}$$

where ψ is defined as

$$q(r,z) = \psi(r,z)\exp(ik_a r) \tag{10}$$

The approximation of the square-root operator Eq. (4) by

$$H_1(z) = k_a\frac{1+\frac{3}{4}s}{1+\frac{1}{4}s} \tag{11}$$

yields the wide-angle PE

$$\left(1+\frac{1}{4}s\right)\partial_r\psi=\frac{1}{2}ik_a s\psi \tag{12}$$

The current paper uses the wide-angle PE given in Eq. (12).

To solve Eq. (9) or (12), the numerical domain needs to be discretized. For example, the vertical grid is uniformly discretized as follows

$$z_j = j\triangle z \quad \text{with j=1,2,...,M} \tag{13}$$

The application of the Crank-Nicholson approximation to Eq. (9) or (12) with the second order finite difference scheme results in a matrix form

$$M_2\vec{\psi}(r+\triangle r) = M_1\vec{\psi}(r) \tag{14}$$

where

$$\begin{aligned} M_1 &= 1+\frac{1}{2}\triangle r(\gamma T+D)+\frac{\gamma T+D}{2ik_a} \\ M_2 &= 1-\frac{1}{2}\triangle r(\gamma T+D)+\frac{\gamma T+D}{2ik_a} \end{aligned} \tag{15}$$

for the wide-angle PE where $\gamma=\alpha/(\triangle z)^2$ and $\alpha=\frac{1}{2}i/k_a$.

The tri-diagonal matrix T is given as

$$T=\begin{pmatrix} -2+\sigma_1 & 1+\sigma_2 & & & & \\ 1 & -2 & 1 & & & \\ & 1 & -2 & 1 & & \\ & & \ddots & \ddots & \ddots & \\ & & & 1 & -2 & 1 \\ & & & & 1+\tau_2 & -2+\tau_1 \end{pmatrix} \tag{16}$$

where the coefficients σ_1 and σ_2 depend on the ground impedance and τ_1 and τ_2 depend on the boundary condition at the top boundary. Therefore, the T matrix includes the effect of ground reflection and air impedance boundary condition at the top.

The diagonal matrix D is given as

$$D = \begin{pmatrix} \beta_1 & & & & & \\ & \beta_2 & & & & \\ & & \beta_3 & & & \\ & & & \ddots & & \\ & & & & \beta_{M-1} & \\ & & & & & \beta_M \end{pmatrix} \tag{17}$$

where $\beta = \frac{1}{2}i(k^2 - k_a^2)/k_a = \frac{1}{2}i\delta k^2/k_a$. The speed of sound at each grid point determines the wavenumber k and, in turn, the value of β. Therefore, the D matrix describes the effect of the variation in the speed of sound.

For a single profile of the speed of sound and the constant ground impedance, the T and D matrices or M_1 and M_2 are calculated once at the initial propagation distance, and then they are used at subsequent propagation distance steps. If the ground impedance changes over the distance, the T matrix, or the M_1 and M_2 matrices should be updated at each distance or range step. If the speed of sound changes over the distance as in the case of evolving wake flows, the D matrix, or the M_1 and M_2 matrices should be updated at each distance or range step.

The boundary condition at the ground is determined using the impedance boundary condition

$$\left(\frac{p_c}{v_{c,n}}\right)_{\mathrm{z=0}} = Z\rho c \tag{18}$$

where Z is the normalized impedance of the locally reacting ground surface, ρc is the impedance of air, p_c is the complex pressure amplitude, and $v_{c,n}$ is the normal component of the complex fluid velocity amplitude. In the current method, the ground impedance (Z) is determined by Delany and Bazley's empirical model[30] whose main unknown parameter is the flow resistivity. The limitation of this model was presented in the literature[8].

If we use the linearized momentum equation

$$v_{c,n} = -\frac{1}{i\omega\rho}\frac{\partial p_c}{\partial z} \tag{19}$$

Eqs (18) and (19) with the second-order finite difference scheme provide the pressure relation

$$p_0 = \left(3 - \frac{2ik_0\triangle z}{Z}\right)^{-1}(4p_1 - p_2) \tag{20}$$

This equation gives the coefficients of σ_1 and σ_2 in Eq (16).

At the top surface at $z = z_M$, the normalized impedance of air ($Z = 1$) is used.

$$p_{M+1} = (3 - 2ik_0\triangle z)^{-1}(4p_M - p_{M-1}) \tag{21}$$

This equation gives the coefficients of τ_1 and τ_2 in Eq (16). The absorbing surface is added to the top boundary in order to prevent artificially reflecting waves from entering the main computation domain. An absorbing surface is positioned $z_M < z <= z_t$ and the imaginary component of the wavenumber $iA_t(z - z_t)^2/(z_M - z_t)^2$ is used. The parameter z_t denotes the upper boundary of the entire computation domain while z_M denotes the boundary before the absorbtion is applied. Therefore, the solution is meaningful below the z_M boundary. The optimum value of A_t is a function of frequency. $A_t = 1, 0.5, 0.4, 0.2$ are used at frequencies of 1000, 500, 125, 30 Hz, and the linear interpolation is used for intermediate frequencies.

The starting field is given by a Gaussian function

$$q(0,z) = S\sqrt{ik_a}\exp(-\frac{1}{2}k_a^2 z^2) \tag{22}$$

where S is a constant that is related to the source strength. For wind turbine noise applications, this constant, S, is found from the sound power level. The method to obtain the sound power level will be introduced in the next sub-section. The conversion is given as

$$S = P_{\text{ref}} \times \sqrt{\frac{10^{L_W/10}}{2\pi}} \tag{23}$$

where $p_{\text{ref}} = 2 \times 10^{-5}$ Pa is the reference sound pressure and L_W is the sound power level. The detailed derivation of Eq. (23) can be found in the Appendix.

For the source above the ground,

$$q(0,z) = q_0(z - z_s) + Cq_0(z + z_s) \tag{24}$$

is used, where z_s is the source location and C is a reflection coefficient. The plane-wave reflection coefficient for normal incidence is used

$$C_p = \frac{Z-1}{Z+1} \tag{25}$$

B. Noise Emission and Source Representation

In wind turbine noise prediction and measurment practice, the *apparent sound power level* is often used to describe the noise source. In this approach, the measured sound pressure level at a reference location in accordance with IEC 61400-11[13] is converted to the sound power level of an imaginary point monopole source at the hub center. The "apparent" emphasizes that it is not the true noise source but the power as "seen" in the measured direction[24]. The conversion of the apparent sound power level from the sound pressure level is given as

$$L_W = L_{p,A} - 6 + 10\log(4\pi R^2/S_0) \tag{26}$$

where L_W is the apparent sound power level, $L_{p,A}$ is the background-corrected, A-weighted sound pressure level at the reference location, R is the slant distance from the rotor centner to the microphone, and S_0 is the reference area that is 1.0. A value of -6 is due to the ground reflection effect. The apparent sound power level is given as one-third octave or octave bands.

In the current PE method, this apparent sound power concept is used. The wind turbine noise source is approximated as a single point monopole source at the hub height and the power levels are given at the octave band central frequencies. There is no doubt that this simple source description does not represent the real source effects of wind turbine noise. In reality, the noise source is moving with a directivity. These effects are not included in the current paper. Recently, the effects of source motion[9;10;16] and the directivity[32] on long-range sound propagation have been studied and these effects can be considered in the future study. However, the validity of the use of a stationary point monopole source in the wind turbine noise was examined in the literature.[23]

C. Attenuation Mechanisms

For long-range propagation of sound, there are several mechanisms to modify the sound including geometrical spreading, atmospheric absorption, ground absorption, and meteorological effects due to wind and temperature gradients. The sound pressure level can be written as,

$$L_p(f_c) = L_W(f_c) - 10\lg(4\pi r^2) - \alpha(f_c)r + \triangle L(f_c) \tag{27}$$

where L_p is the sound pressure level at the observer, L_W is the sound power level at the source, r is the propagation distance, f_c is the central frequency of broadband spectra, α is the atmospheric absorption coefficient, and $\triangle L$ is the relative sound pressure level. The atmospheric absorption[2;3;14] are simply calculated by an analytical formula. The geometric spreading is accounted for the PE method via the envelope function so that it shouldn't be calculated independently. The relative sound pressure ($\triangle L(f_c)$) quantifies the sound refraction and ground absorption effects: it is a useful metric to show the sound propagation effects due to wind and temperature variations (long-term deterministic or short-term stochastic variations).

III. Validation of the Parabolic Equation Method

To validate the PE method, comparisons are performed first with an analytic solution, secondly with benchmark problems, and finally with far-field noise experimental data.

A. Analytic Solution

A point monopole source with PWL of 100 dB and a frequency of 125Hz is positioned at 10m above an acoustically hard surface. Above 100m of height, an absorbing surface of a height of 30 times the wavelength is added to dissipate acoustic pressure. For this analytic solution, there is no spatial variation of the speed of sound. Figure 1 shows the SPL contours above the ground. The constructive and destructive interference patterns between the direct sound propagation and reflected sound propagation by the ground generate multiple lobes. It is shown that the sound waves are dissipated in the absorbing area and no artificial reflections from the top surface exist. Figure 2 shows a comparison between the analytic solutions and the PE results for SPL and the real part of the acoustic pressure at a height of 2m above the ground. The PE results are shown to be in good agreement with analytic solutions. A small deviation near the source is due to the inherent limitation of the PE to shallow propagation angles.

In order to investigate the effect of the source height and to simulate a realistic wind turbine noise source location, the source is placed 80m above the hard ground. The source frequency and power level are the same as in the 10m source height case. Figure 3 shows a comparison of the SPL and the real part of the acoustic pressure at 2m above the ground between analytic solutions and CNPE results. The agreement between the analytic solutions and the PE results is excellent beyond 100m of propagation distance, which corresponds to about 40 deg of the elevation angle. Note that for modern large wind turbines of 1-2MW rated power with large blades and tall towers, it would be acceptable to rely on the PE results beyond 100m.

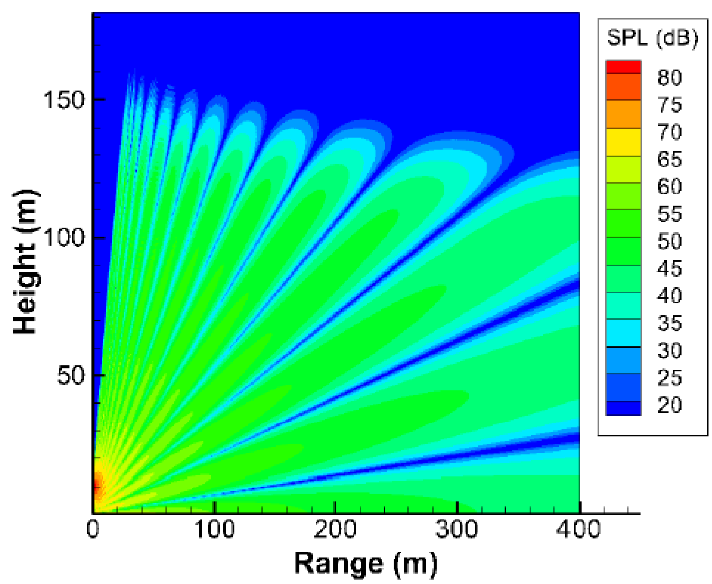

Figure 1. Sound pressure contours for a source of 100dBA PWL at 125Hz positioned at 10m above acoustically hard surface.

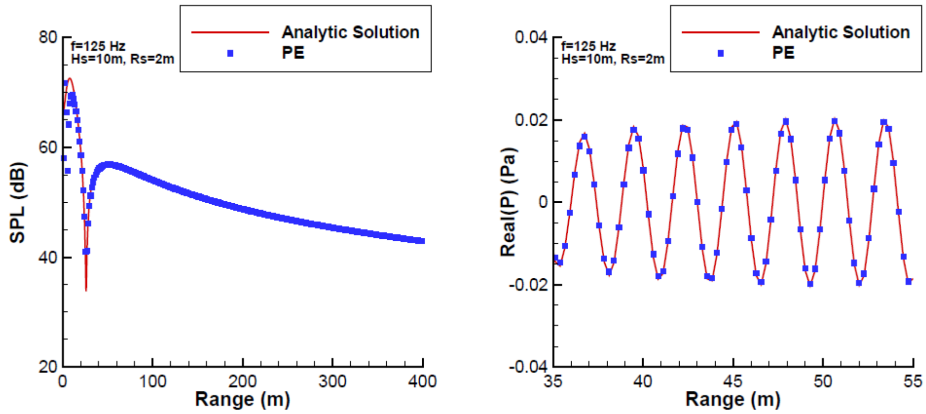

(a) (b)

Figure 2. **Comparison between analytic solutions and the CNPE results computed at 2m above the ground for a source of 100dBA PWL at 125Hz which is positioned at 10m above an acoustically hard surface: (a) SPL, (b) real part of the acoustic pressure**

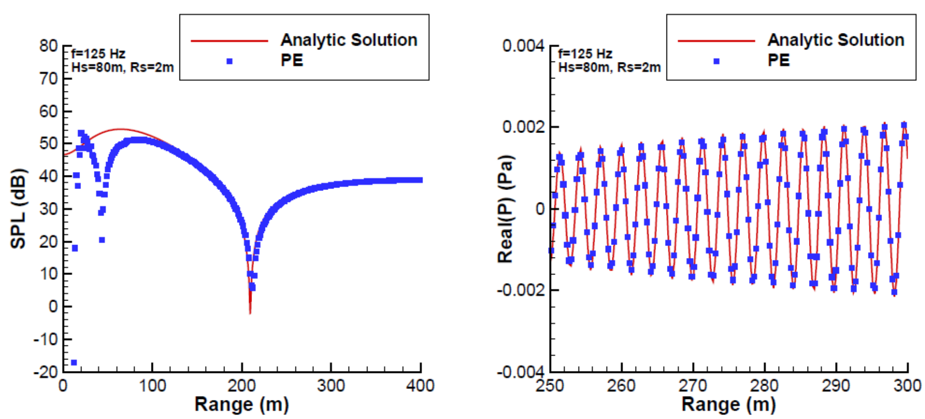

(a) (b)

Figure 3. **Comparison between analytic solutions and the CNPE results computed at 2m above the ground for a source of 100dBA PWL at 125Hz which is positioned at 80m above an acoustically hard surface: (a) SPL, (b) real part of the acoustic pressure**

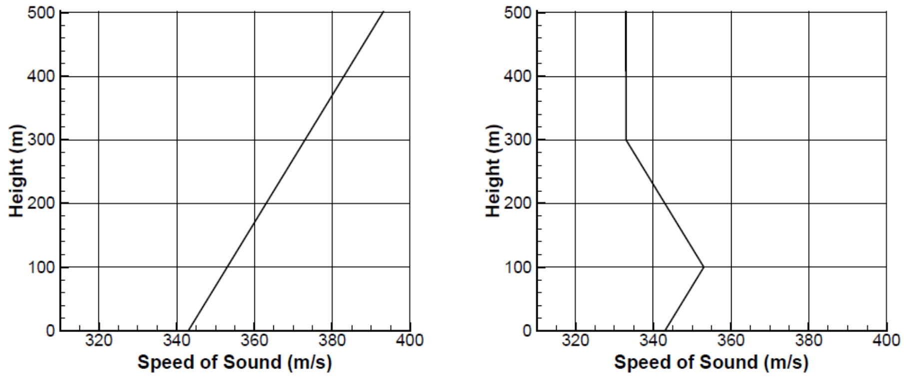

(a) (b)

Figure 4. Speed of sound profile for the test cases: (a) Case 2 (downwind condition), (b) Case 4 (composite profile)

B. Benchmark Problems

In order to verify the PE code for non-constant speed of sound profiles, the current PE method is compared with benchmark problems for outdoor sound propagation models[1]. The source and receiver heights are 5m and 1m, respectively. The frequency is 100Hz and the ground impedance is 12.81+i11.62. The sound velocity at the surface is 343 m/s. The transmission loss, $20\log(p/p_0)$, is used to evaluate the accuracy of the tool, where p is the acoustic pressure at the receiver and p_0 is the pressure at the source location. Although there are four benchmark cases presented in reference[1], only two cases, a strong positive sound speed gradient simulating a downwind condition (case 2) and a composite sound speed profile (case 4), are considered in the current paper. The profiles of the speed of sound for these two cases are shown in Fig. 4. Case 2 uses a linear profile with a constant gradient of $0.1s^{-1}$. In case 4, the profile starts at the surface with a positive constant gradient of $0.1s^{-1}$ up to a height of 100 m and then the gradient becomes a constant value of -$0.1s^{-1}$ up to a height of 300 m. From this point on the sound speed remains constant.[1].

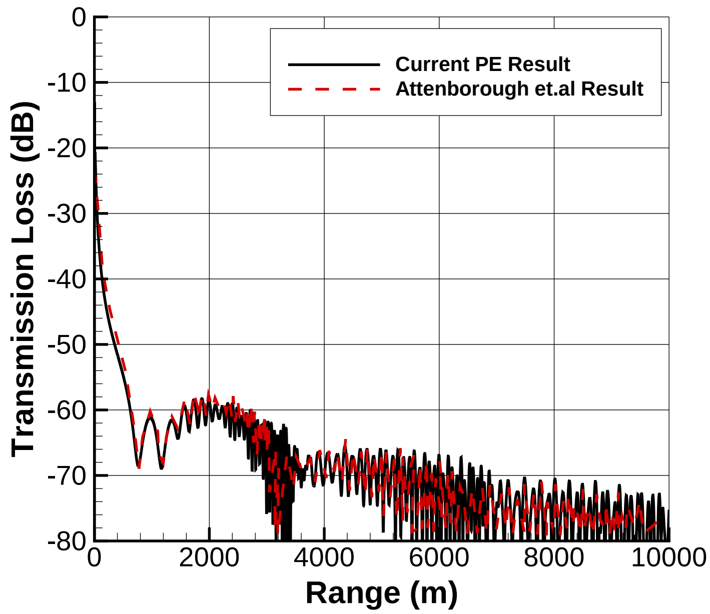

Figure 5. Transmission loss versus range for case 2 with a frequency of 100Hz

Figure 5 shows the transmission loss versus range up to 10km for case 2. It can be seen that the current PE method yields almost the same result with the benchmark result. Complex patterns of dips and peaks are well captured in the current model. Figure 6 shows the transmission loss for case 4. Again, the level and shape of the transmission loss obtained by the current PE method agree very well with the benchmark results. Figure 7 shows the relative sound pressure level contours predicted by the current PE for case 2 and case 4. The downwind refraction and caustic lines are shown in the figures.

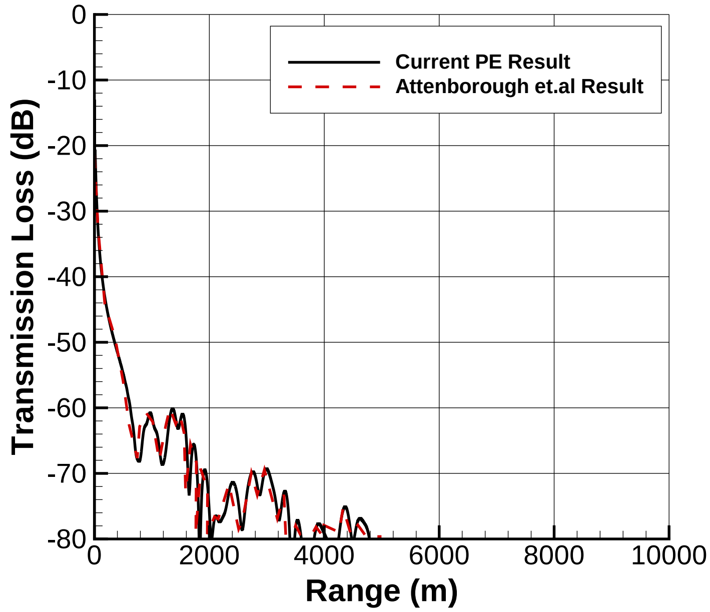

Figure 6. Transmission loss versus range for case 4 with a frequency of 100Hz

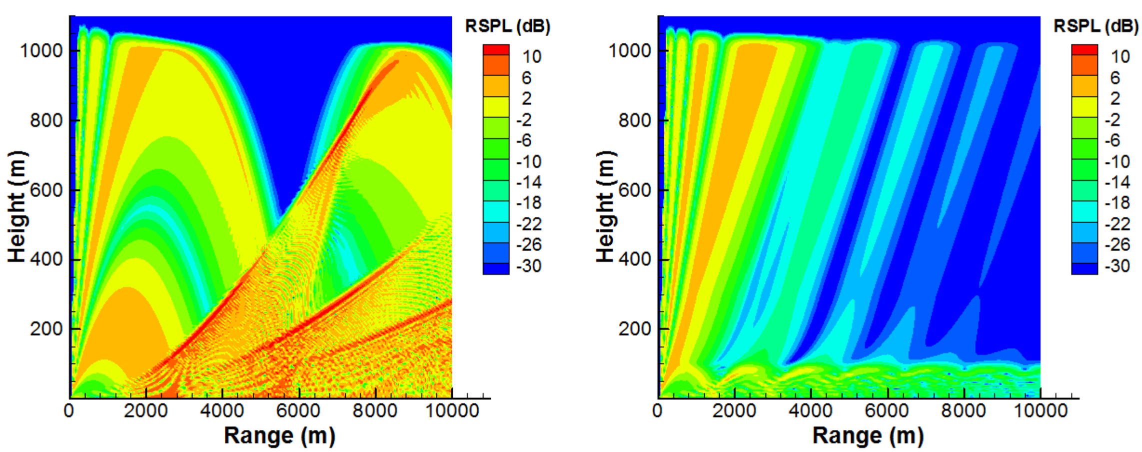

Figure 7. Relative sound pressure level contours predicted by the PE model for (a) case 2, (b) case 4

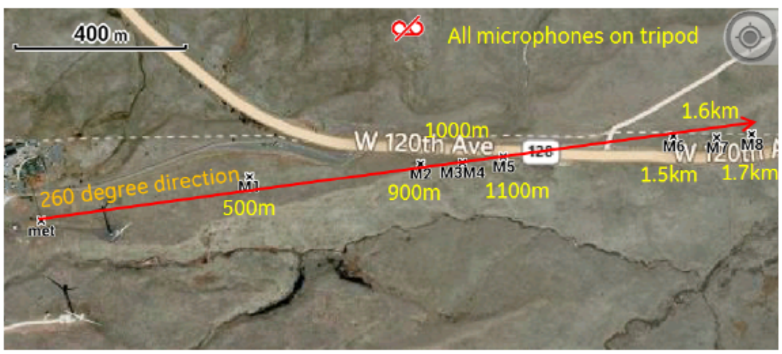

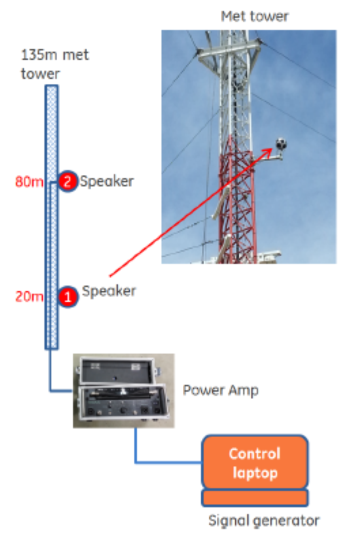

(a) (b)

Figure 8. Noise validation study: (a) microphone layout, (b) speaker positioned at met tower

C. Far-Field Sound Measurement

The PE code results are now compared with far-field sound experimental data. The data were collected at the National Wind Technology Center (NWTC) of the National Renewable Energy Laboratory (NREL) in Colorado. A B&K omni-directional speaker that generates pure tone sound was located either at 20m or 80m height on a meteorology mast. The pure tone is narrow band and the tone frequencies are 125Hz, 250Hz, 500Hz, and 1kHz. Seven microphones were located at 2m above the ground. The microphones are B&K outdoor microphone with a wind shield. The distances of the microphones from the met tower are 500m, 900m, 1km, 1.1km, 1.5km, 1.6km, and 1.7km, respectively. Sound recording hardware is B&K 2250 with sound recording. Two wind directions were used to investigate the propagation effect: downwind propagation and upwind propagation. Given the layout of the microphones, the downwind direction is southwest and the upwind propagation direction is northeast. Figure 8 shows the microphone locations and the speaker positioned at the met tower. The site has a relatively flat topography. However, at high frequencies such as 500Hz and 1kHz where the wavelengths are less than 1m, the flat topography may not be an accurate assumption and a complex topography modeling would provide more accurate results.

The meteorology mast recorded the wind speed, wind direction, temperature at 10m, 38m, and 87m heights. The effective sound speed gradient can be calculated from the 5 minute averaged wind and temperature data. The measured sound data were recorded every 5 minutes at the frequencies of interest. The 5 minute periods just before and just after the period that the loudspeaker emits a tone at a specific frequency are used to determine the background sound for that 5 minute data point. For example, if the

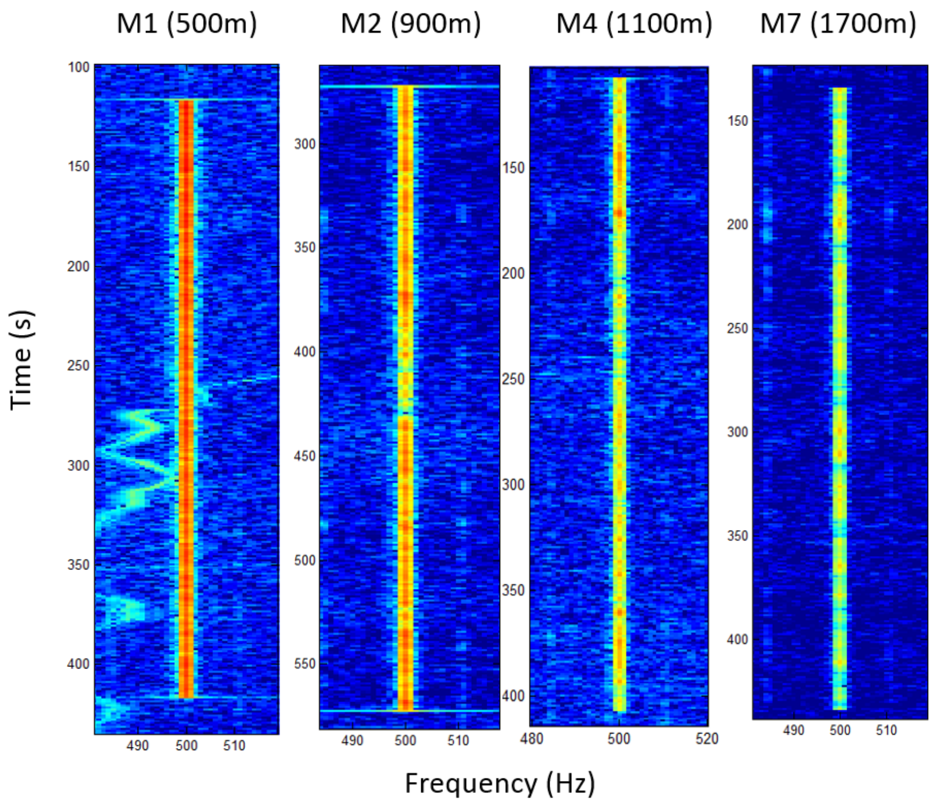

Figure 9. Contour of measured tonal sound at various microphone locations. The tonal sound is emitted from a 20m height speaker at 500 Hz.

loudspeaker emits sound at 500Hz from 10:05 to 10:10, then the sound levels at 125Hz from 10:00-10:05 and from 10:10 to 10:15 are used to determine the background sound. At those times the loudspeaker may emit a different pure tone, but this does not impact the measured sound at 500Hz. This technique provides a very good signal-to-noise ratio even at far distances. Figure 9 shows the speaker tonal sound variation at multiple microphone locations. The tonal sound was generated by a 20m height speaker and the tone frequency is 500Hz. It is shown that that the tonal sound is well captured even at far distances compared to background noise.

Figure 10 shows a comparison of sound results between the measurements and PE results at each test frequency for a speaker of 20m height. The standard deviation of the measured sound and background sound are also included in the plots. The measured background sound is added to the PE results so that unrealistic large sound dips that can be predicted by PE are avoided. The figure shows the downwind and upwind sound propagations at all frequencies. The wind shear exponent is added in the figure caption.

It is seen that the measurement shows an increase in the sound levels at further distances in some cases in the downwind propagation. This is believed to be due to the sound refraction effects and the PE provides a similar behavior. It is seen that the measured sound is significantly reduced beyond 1km in the upwind propagation. The PE also provides very low sound levels in the upwind propagation. It is promising that the PE differentiates the effect of the propagation direction and provides similar trends with the measurement. Since the current PE does not include atmospheric turbulence effects that scatters acoustic energy into the sound shadow zone, however, the sound reduction is overestimated in the sound shadow zone. It is suggested that the validation test be repeated with the PE model after including the turbulent scattering effects in the future.

Figure 11 shows the same results but with the speaker of 80m height. The PE method provides good agreement with the measurement in the downwind propagation and underpredicts the sound levels in the upwind direction due to the lack of the turbulence scattering of sound energy into the sound shadow zone. Important lessons from this measurement study are that the sound propagation can be very different depending on the propagation direction and the turbulent scattering effect should be included in the PE method in order to accurately predict sound propagation in the upwind direction.

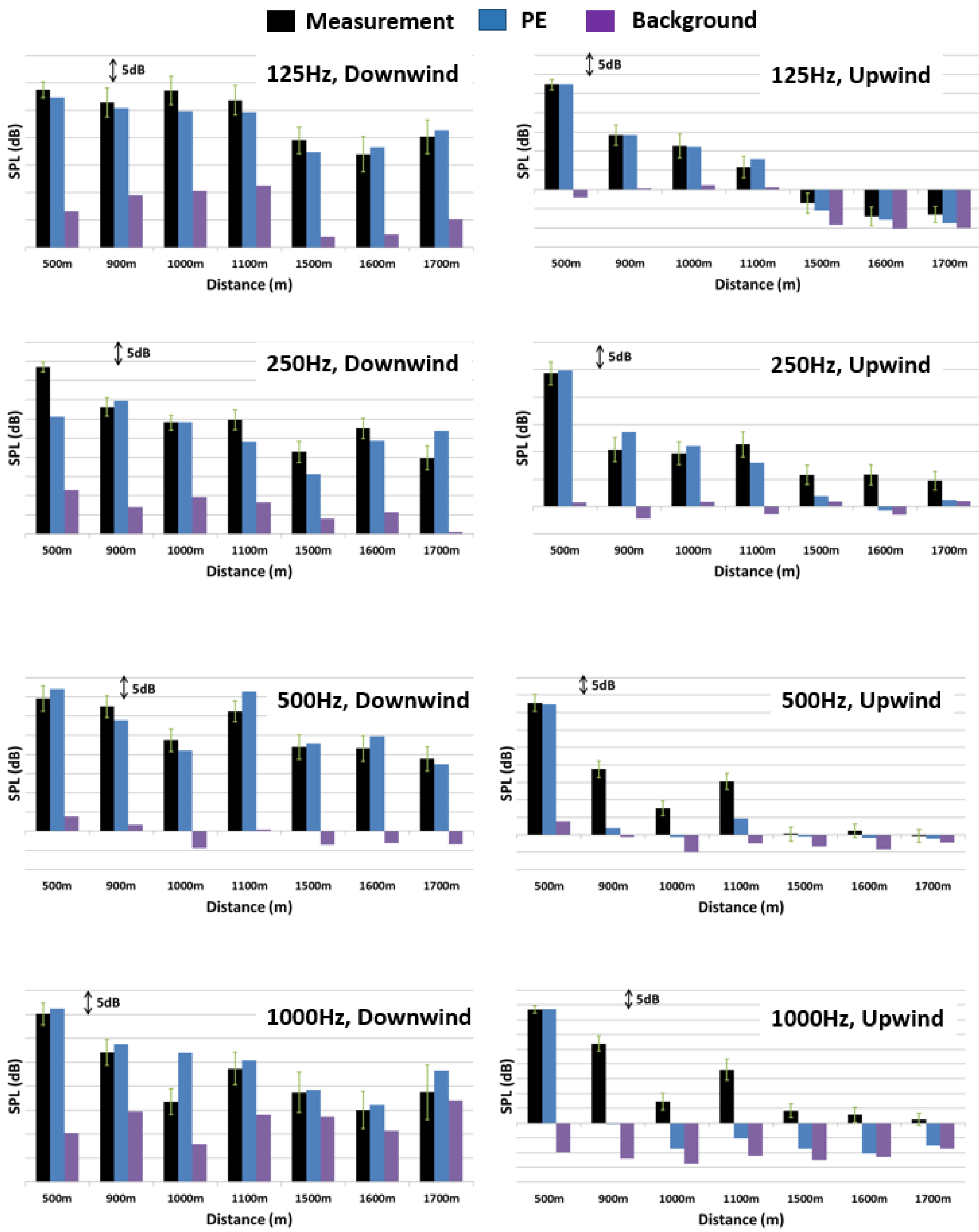

Figure 10. Prediction comparison against measured data for sound propagation validation study with a 20m source (a) 125Hz downwind (WS=0.27), (b) 125Hz upwind (WS=0.18), (c) 250Hz downwind (WS=0.53), (d) 250Hz upwind (WS=0.37), (e) 500Hz downwind (WS=0.07), (f) 500Hz upwind (WS=0.37), (g) 1000Hz downwind (WS=0.08), and (h) 1000Hz upwind (WS=0.48)

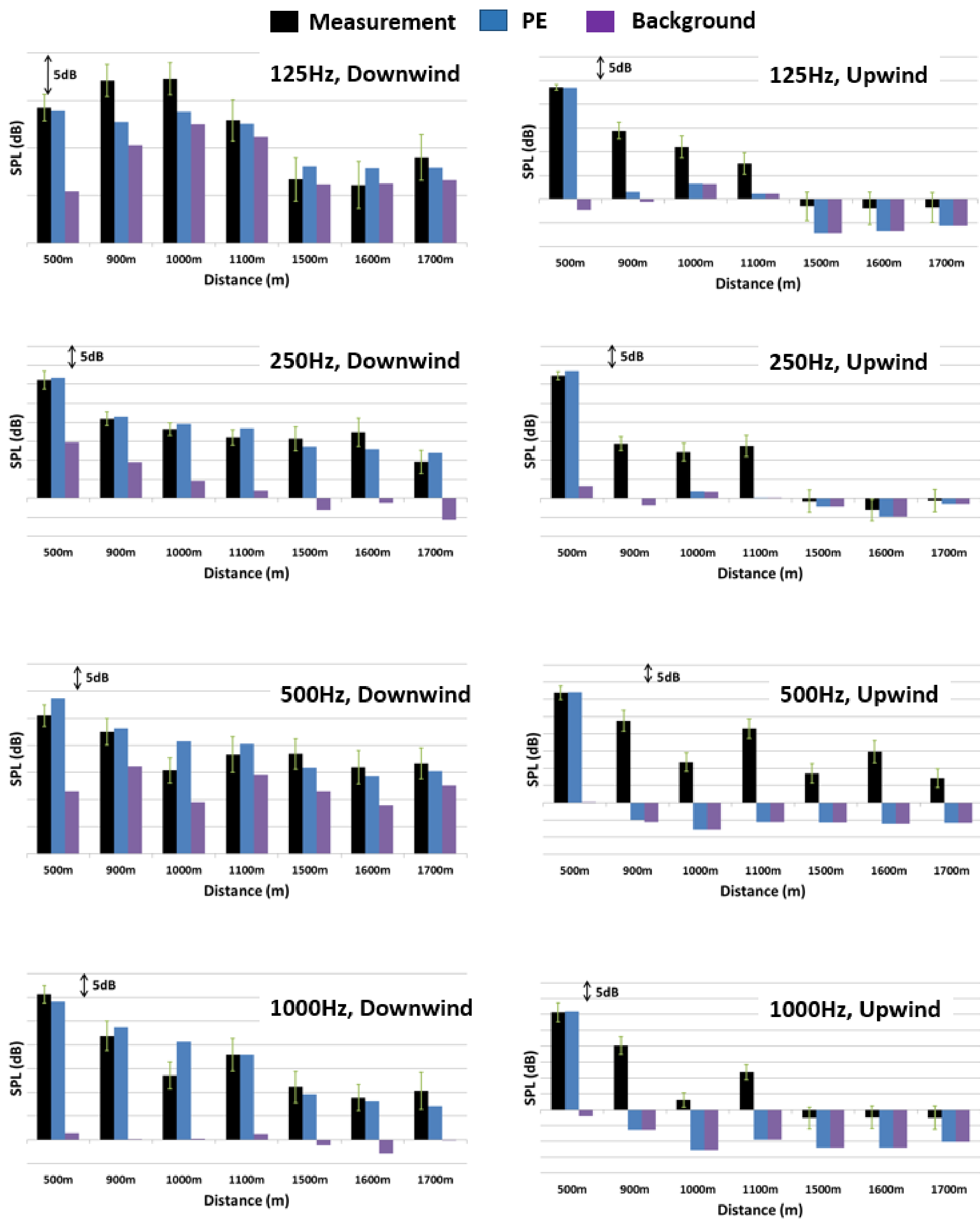

Figure 11. Prediction comparison against measured data for sound propagation validation study with a 80m source (a) 125Hz downwind (WS=0.19), (b) 125Hz upwind (WS=0.42), (c) 250Hz downwind (WS=0.12), (d) 250Hz upwind (WS=0.26), (e) 500Hz downwind (WS=0.09), (f) 500Hz upwind (WS=0.64), (g) 1000Hz downwind (WS=0.06), and (h) 1000Hz upwind (WS=0.63)

IV. Wind Turbine Sound Propagation with Wake Flows

Now that the PE model has been verified with analytic solutions, benchmark problems, and experimental data, it is applied to realistic wind turbine noise propagation in this section. In particular, sound speed profiles and the associated sound propagation can be significantly modified by turbine wake flows in the downwind direction. The sound speed profiles are determined by the local temperature and wind speed or the effective speed of sound[30], $c = \sqrt{\gamma RT} + u$, where γ is the specific heat ratio, R is gas constant, T is the temperature (K), and u is the wind velocity (m/s) in the propagation direction. If the wind velocity is not aligned with the propagation direction, the angle between the mean wind direction and the propagation direction should be accounted for. Assuming incompressible and adiabatic conditions, the speed of sound is directly changed by the local wind speed that is in turn influenced by the wake flows in the downwind direction. However, the understanding of the effect of the wake flows on wind turbine noise propagation is limited.

The PE code uses the RANS CFD results as input to compute sound propagation with more detailed wind velocity profiles for wake flows. An actuator disk (AD) model[5;29], which is an efficient tool to capture turbine wake flows, is implemented into ANSYS CFX. The AD treats the forces on the blades as body forces acting on the fluids. The validity of the actuator disk model and its comparison with the measured wake profile is shown in the literature[5]. Please note that this simple model only provides the mean shear profile in the vertical direction and the mean swirl effect is not captured. However, this model is consistent with the 2-D assumption of the current PE model.

The source model is the apparent sound power level as discussed in section II. B. The monopole source is located at the rotor center and the broadband noise level is prescribed at the octave band central frequencies. The absolute noise level is not of significant interest. The paper focuses on the relative importance of the effect of wake flow on the noise propagation.

Figure 12 shows the AD CFD domain. The AD source region is highlighted in the figure. The entire CFD domain size is 40 times the rotor diameter in the streamwise direction and 4 times the rotor diameter in the cross-wind direction. A finer mesh is used near the AD region and the mesh is clustered at the blade root and tip regions. The streamwise grid spacing in the AD region is $0.0065D$ where D is the rotor blade radius. The total mesh size is 9M nodes.

The atmospheric boundary layer is characterized by the friction velocity (U^*) and the aerodynamic roughness length y_0.

$$U = \frac{U^*}{k} \ln\left(\frac{y + y_0}{y_0}\right) \tag{28}$$

where $k = 0.41$ is the von Karman constant. The boundary condition on the bottom surface is that of a rough wall with a sand grain roughness height K_s. A large value of the roughness height is desired to maintain the freestream wind profile up to the exit of the CFD domain, but it should be smaller than the first cell height too. The optimal value of the roughness height is found from free shear CFD runs without the turbine actuator disk model. The boundary condition on the top surface is the the smooth wall boundary condition with a specified shear in the streamwise direction that generates the appropriate atmospheric boundary layer. The specified shear in the streamwise direction is $\rho U^{*2}/2$ where ρ is the flow density.

Turbulent kinetic energy and eddy viscosity ratio are important in terms of the mixing of turbulent wake flows and the transition from near-wake to far-wake. The

Table 1. Parameters for actuator disk CFD runs

U^*	y_0	K_s	C_1	C_2	Case
1.0	1	5	0.01	0.01	Day
2.7	20	5	0.005	0.005	Night
4.5	40	5	0.001	0.001	Large
8.0	100	8	0.0005	0.0005	Extreme

turbulent kinetic energy and eddy viscosity ratio are given as

$$TKE = C_1 \frac{U^{*2}}{\sqrt{C_\mu}} \tag{29}$$

$$\epsilon = C_2 \frac{U^{*3}}{k(y+y0)} \tag{30}$$

where C_1 and C_2 are the scaling constants. Four cases, designated as *Day, Night, Large, and Extreme* according to their wind shear, are generated to test sound propagation, and Table 1 shows the parameters for these cases that are determined from free shear CFD runs. For all cases, the freestream velocity at the hub height is approximately the same.

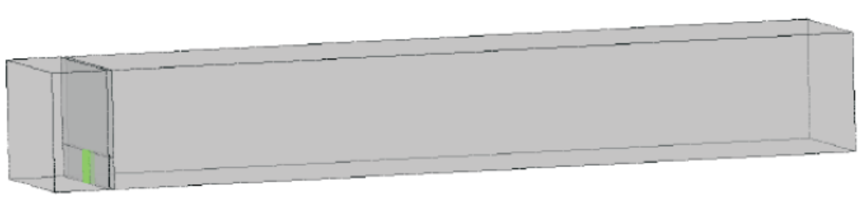

Figure 12. Actuator disk CFD domain

Figure 13 shows the velocity contours in the vertical plane for four cases. The development and mixing of shear flows are observed in the downstream direction. Figure 14 shows more quantitative wind velocity profiles that are extracted from the results shown on Fig. 13 for four cases at multiple streamwise distances. It is shown that the velocity profiles at the right turbine location have two peaks. These peaks merge further downstream due to the mixing of freestream turbulence, which generates one bigger peak at around $4D$. This peak amplitude is reduced further downstream and the velocity profiles approach to the freestream velocity but with a smaller velocity magnitude. Overall, the wake flow significantly modifies the velocity profile as a function of the propagation distance and the vertical height. A steep gradient of the local wind profile is more obvious in the lower wind shear case. As the wind shear increases, the wind profiles resemble more the freestream velocity profile, but still have local complex profiles. These complex wake flows are expected to have significant impacts on sound propagation through local upwind (negative velocity gradient) and local downwind (positive velocity gradient) conditions. This local variation of wind profiles acts as an acoustic channel that carry the acoustic energy.

Figure 15 shows the overall sound pressure levels as a function of propagation distances for four conditions. The PE was simulated at the octave band central frequencies up to 1kHz and then the sound pressure levels were combined to generate the overall sound pressure levels. Each plot contains the simple wind shear results (without wake) and the results with wake flows superimposed on the wind shear (with wake). For a small wind shear case (a), the wake flows tend to increase the far-field noise levels. As the wind shear increases, the far-field noise levels are reduced in the presence of wake flows. This finding is somewhat different from the conclusion of Heimann, et al.[12] that claims that wake flows increase the noise levels at large distances. Note that the simulation of Heimann, et al. [12]

is limited to 1km of distance and one wind shear condition. It appears that a large change in the noise levels due to wake flows occur beyond 1.5km. It is also shown that the effect of wake flows depends on the wind shear. Overall, wake flows redistribute the acoustic energy and modify the propagation characteristics. However these effects might be limited to a very narrow corridor only in the downwind direction where wake flows are dominant. In addition, the signal-to-noise ratio may not be large enough to detect the difference at large distances. An experimental investigation should be conducted to find out the effect of wake flows on sound propagation in real life.

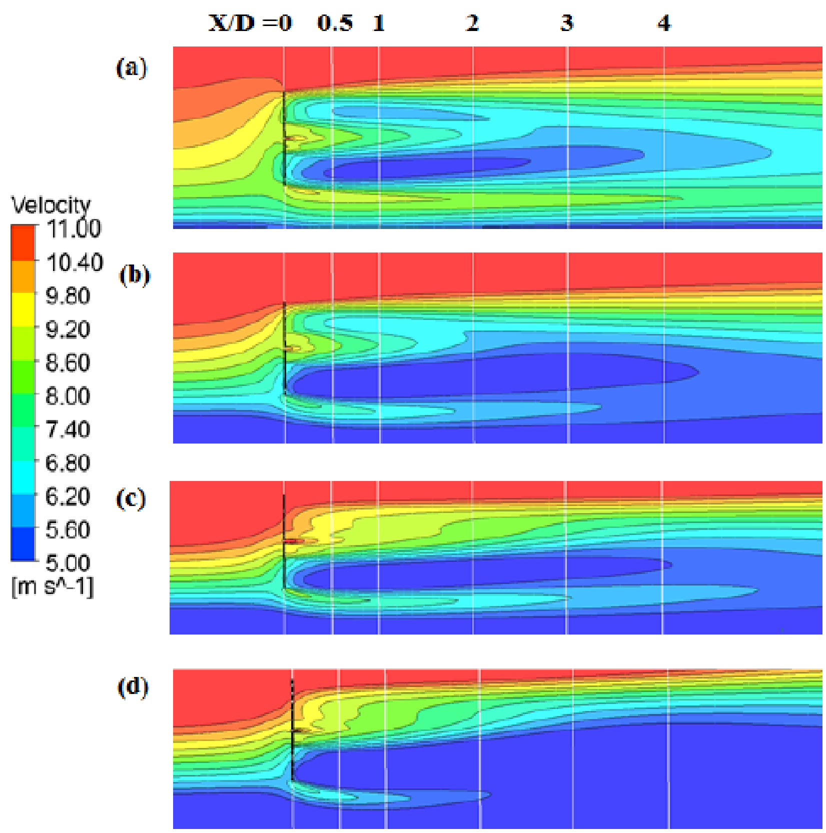

Figure 13. Wind velocity contours in the vertical plane with the actuator disk: (a) Day, (b) Night, (c) Large, (d) Extreme. (The vertical scale is $Z(m)$.)

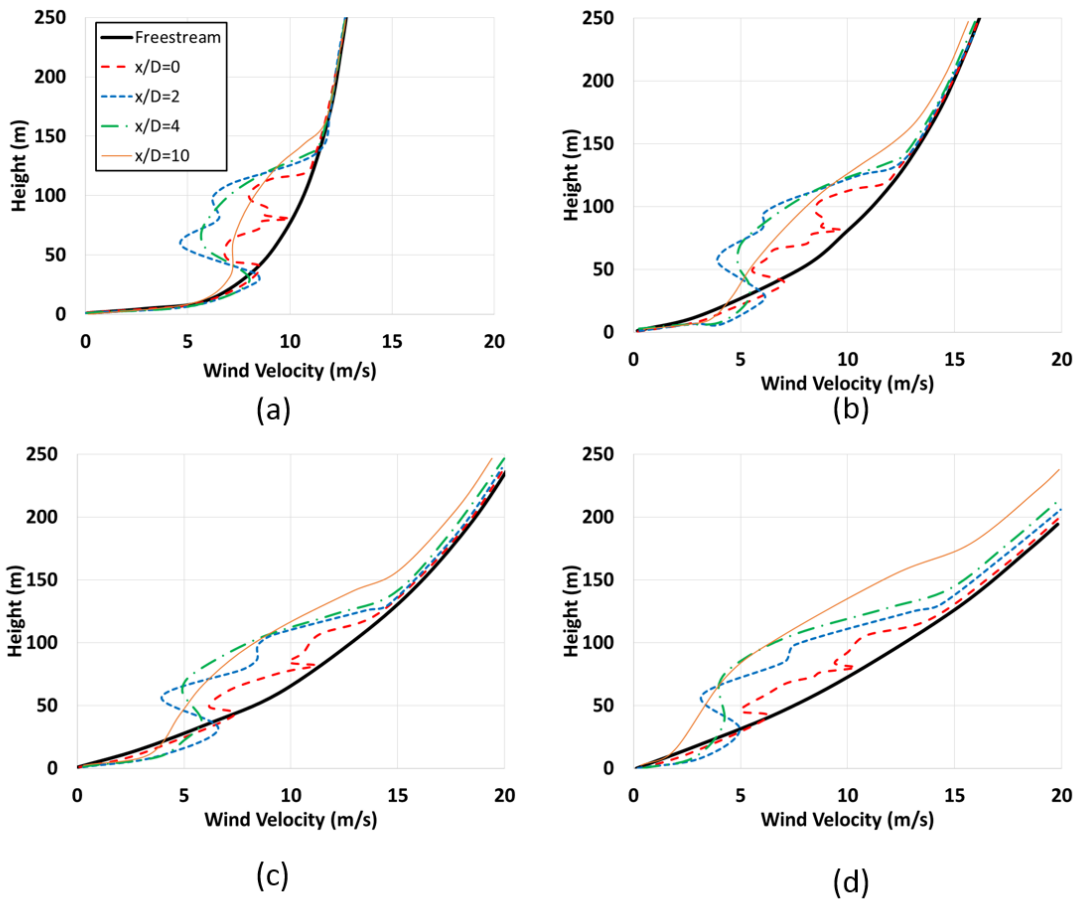

Figure 14. Wind velocity profiles with the actuator disk: (a) Day, (b) Night, (c) Large, (d) Extreme

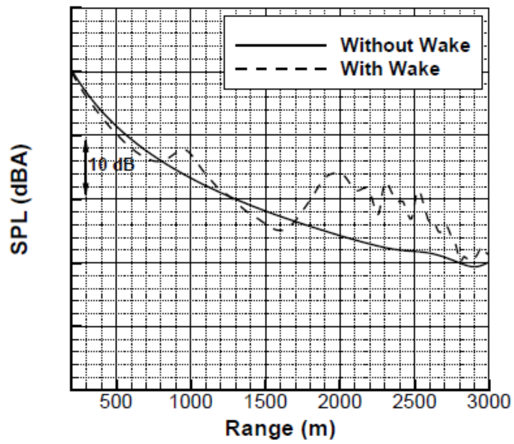

(a)

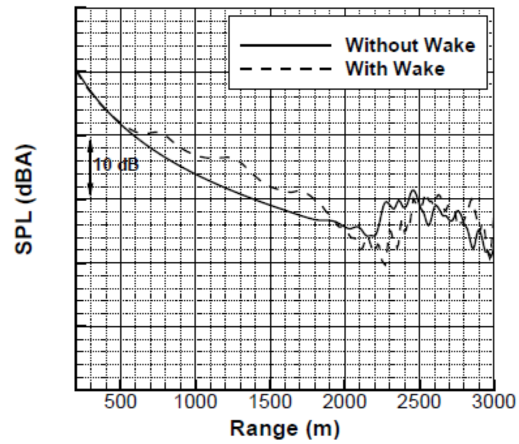

(b)

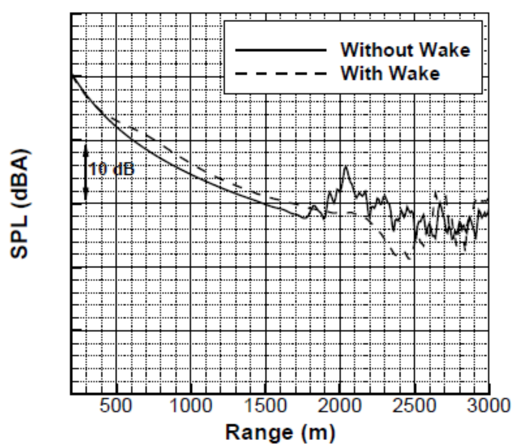

(c)

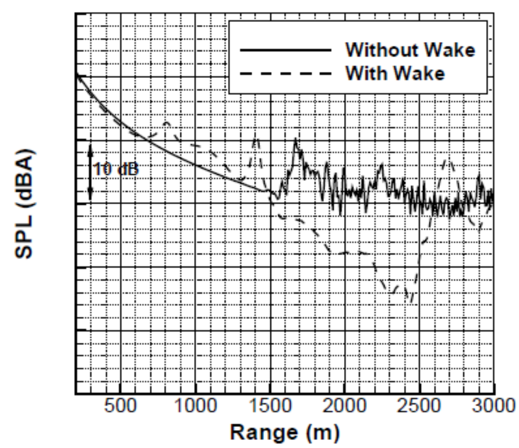

(d)

Figure 15. Overall sound pressure levels with and without wake flows: (a) Day, (b) Night, (c) Large, (d) Extreme

V. Conclusions

In this paper, the PE method was developed for applications to wind turbine noise propagation and it was extensively validated with analytic solutions, benchmark problems, and far-field experimental data. Far-field experimental data showed that, in the downwind direction, sound levels do not monotonically decrease due to refraction effects and that the far-field sound levels can be very different depending on the propagation direction as expected. The current PE method under-predicted the noise levels at far-field in the upwind direction due to the lack of turbulence scattering effect.

The PE method used CFD results as input to predict sound propagation with evolving wake flows. CFD provides the detailed wake flows or velocity profiles that vary as a function of the distance and height. It was shown that turbine wake flows significantly modify the sound propagation characteristics that depend on the wind shear and propagation distance.

The current PE model used an apparent sound power level in which a point monopole source is located at the rotor center and the octave band central power levels are used. Although this is a standard practice in wind industry, it is a too simplified assumption. In order to consider realistic wind turbine noise source, it is suggested to include the effects of the directivity and the source motion and to find out a direct connection between the source description in the PE model and the turbine blade trailing edge noise generation as a function of frequency.

The current PE model is limited to 2D propagation, flat ground and non-turbulent atmosphere. Even though it is possible to extend the tool capability to account for 3D propagation, complex terrains, turbulent atmosphere, there are many other challenges in the prediction of sound propagation. The prediction depends on the input of wind and temperature profiles. This information may not be easily obtainable in real situations. It requires additional meteorological measurement equipments in the field. Statistical predictions or uncertainty quantifications are also useful since they provide the mean and variance of far-field noise levels. The uncertainties due to sound source description, such as temporal or dynamic effects and 3D effects, PE limitations, the accuracy of CFD calculations also should be investigated.

VI. Acknowledgments

The authors would like to thank Sachin Premasuthan (GE Global Research) for providing the RANS actuator disk model to compute the wake flows. The authors are also grateful to Benoit Petitjean, Roger Drobietz, Kevin Kinzie (GE Power), and Thierry Maeder (GE Global Research) for very useful input and discussion.

VII. Appendix

The starting pressure strength constant, S, can be obtained by the sound power level, L_W. The time-averaged sound intensity is written as,

$$I_{av} = \frac{W_{av}}{4\pi R^2} \tag{31}$$

The complex pressure amplitude with the constant S can be written as,

$$p_c = S\frac{\exp(ikr)}{R} \tag{32}$$

Then, the intensity can be expressed with the pressure term for plane waves

$$I_{av} = \frac{(p^2)_{av}}{\rho c} \tag{33}$$

where $(p^2)_{av}$ denotes the averaged pressure square. Equations (31) and (33) provide the constant

$$S = \sqrt{\frac{\rho c W_{av}}{2\pi}} \tag{34}$$

The sound power level is given as,

$$L_W = 10 \lg \left(\frac{W_{av}}{W_{\text{ref}}} \right) \tag{35}$$

where $W_{\text{ref}} = 1 \times 10^{-12}$W is the reference sound power. Then, W_{av} is written as,

$$W_{av} = W_{\text{ref}} \times 10^{L_W/10} \tag{36}$$

The values of p_{ref} and W_{ref} satisfy the relation

$$p_{\text{ref}}^2 \simeq \rho c W_{\text{ref}} \tag{37}$$

where $p_{\text{ref}} = 2 \times 10^{-5}$ Pa is the reference sound pressure. Combining Eqs. (34), (36), and (37) yields

$$S = P_{\text{ref}} \times \sqrt{\frac{10^{L_W/10}}{2\pi}} \tag{38}$$

REFERENCES

Attenborough, K. 1995, "Benchmark Cases for Outdoor Sound Propagation Models," *J. Acoust. Soc. Am*, 97(1), 173–191.

Bass, H., Sutherland, L., Zuckerwar, A., and Blackstock, D. 1995, "Atmospheric Absorption of Sound: Further Developments," *Journal of the Acoustical Society of America*, 97(1), 680–683.

Bass, H., Sutherland, L., Zuckerwar, A., and Blackstock, D. 1996, "Erratum: Atmospheric Absorption of Sound: Further Developments," *Journal of the Acoustical Society of America*, 99(2), 1259.

Bolin, K., and Boué, M. 2009, "Long Range Sound Propagation Over a Sea Surface," *J. Acoust. Soc. Am*, 125(5), 2191–2197.

Castellani, F., and Vignaroli, A. 2013, "An Application of the Actuator Disc Model for Wind Turbine Wakes Calculations," *Applied Energy*, 101, 432–440.

Cheng, R., Morris, P., and Brentner, K. 2009, "A Three Dimensional Parabolic Equation Method for Sound Propagation in Moving Inhomogeneous Media," *J. Acoust. Soc. Am.*, 126(4), 1700–1710.

Dinapoli, F., and Deavenport, R.L. edited by DeSanto, J. 1979, "Numerical Modles of Underwater Acoustic Propagation, Chapter 3 in Ocean Acoustics,".

Dragna, D., Attenborough, K., and Blanc-Benon, P. 2015, "On the Inadvisability of Using Single Parameter Impedance Models for Representing the Acoustical Properties of Ground Surfaces," *Journal of the Acoustical Society of America*, 138(4), 2399–2413.

Dragna, D., and Blanc-Benon, P. 2014, "Towards Realistic Simulations of Sound Radiation by Moving Sources in Outdoor Environments," *International Journal of Aeroacoustics*, 13(5-6), 405–426.

Dragna, D., and Blanc-Benon, P. 2015, "Sound Radiation by a Moving Line Source above an Impedance Plane with Frequency-Dependent Properties," *Journal of Sound and Vibration*, 349, 259–275.

Gilbert, K., and White, M. 1989, "Application of the Parabolic Equation to Sound Propagation in a Refracting Atmosphere," *J. Acoust. Soc. Am.*, 85, 630–637.

Heimann, D., Käsler, Y., and Günter, G. 2011, "The Wake of a Wind Turbine and Its Influence on Sound Propagation," *Meteorologische Zeitschrift*, 20(4), 449–460.

IEC61400-11 2006, "Wind Turbine Generator Systems–Part II:Acoustic Noise Measurement Techniques, 2nd ed.,", International Technical Commission, Geneva, 2002 plus Amendment I 2006.

ISO 9613-1: Acoustics Attenuation of Sound During Propagation Outdoors, Part 1 Calculation of the Absorption of Sound By The Atmosphere 1993*International Standards Organization*, 1–26.

ISO9613-2: Acoustics Attenuation of Sound During Propagation Outdoors, Part 1 General Method of Calculation 1996*International Standards Organization*, 1–24.

Jacob, M. C., Dragna, D., Cahuzac, A., Boudet, J., and Blanc-Benon, P. 2014, "Towards Hybrid CAA with Ground Effects," *International Journal of Aeroacoustics*, 13(3-4), 235–260.

Jensen, F., Kuperman, W., Porter, M., and Schmidt, H. 1994, *Parabolic Equations, Chapter 6 in Computational Ocean Acoustics*, New York: American Institute of Physics.

Johansson, L. 2003 , Sound Propagation Around Off-Shore Wind Turbines: Long-Range Parabolic Equation Calculations for Baltic Sea Conditions, Licentiate thesis, Kungl Tekniska Högskolan. 1-87

Kalapinski, E. 2009, Wind Turbine Acoustic Modeling with the ISO 9613-2 Standard: Methodologies to Address Constraints,, in *Third International Conference on Wind Turbine Noise*, Aalborg, Denmark.

Kaliski, K., and Wilson, K. D. 2011, Improving Predictions of Wind Turbine Noise Using PE Modeling,, in *NOISE-CON 2011*, Portland, Oregon, 1–13.

Lee, D., Pierce, A., and Shang, E. 2000, "Parabolic Equation Development in the Twentieth Century," *J. Acoust. Soc. Am.*, 8, 527–637.

Manning, C. J. 2009, The Propagation of Noise from Petroleum and Petrochemical Complexes to Neighbouring Communities, *CONCAWE*

Makarewicz, R. 2011, "Is a Wind Turbine a Point Source?," *Journal of the Acoustical Society of America*, 129(2), 579–581.

Mø ller, H., and Pedersen, C. S. 2011, "Low-Frequency Noise from Large Wind Turbines," *Journal of the Acoustical Society of America*, 129(6), 3727–3744.

Mylonas, L. 2014, pp. 1–105, Assessment of Noise Prediction Methods over Water for Long Range Sound Propagation of Wind Turbines,, Master's thesis, Uppsala University.

Nota, R., Barelds, R., and van Maercke, D. 2005, "Harmonoise WP 3 Engineering Method for Road Traffic and Railway after Validation and Fine-tuning," *HAR32TR=040922-DGMR20:DGMR*

Prospathopoulos, J. M., and Voutsinas, S. G. 2005, "Noise Propagation Issues in Wind Energy Applications," *Journal of Solar Energy Engineering*, 127, 234–241.

Prospathopoulos, J. M., and Voutsinas, S. G. 2007, "Application of a Ray Theory Model to the Prediction of Noise Emissions from Isolated Wind Turbines and Wind Parks," *Wind Energy*, 10, 103–119.

Réthoré, P.-E., Van der Lann, P., Troldborg, N., Frederik, Z., and Sørensen, N. N. 2013, “Verification and Validation of an Actuator Disc Model,” *Wind Energy*, 17(6), 919–937.

Salomons, E. M. 2001, pp. 1–327, *Computational Atmospheric Acoustics*, Netherlands: Kluwer Academic Publishers.

Tappert, F.D. edited by Keller, J., and Papadakis, J. 1977, “The Parabolic Approximation Method, Chapter 5 in Wave Propagation and Underwater Acoustics,”.

Vecherin, S. N., Wilson, D. K., and Ostashev, V. E. 2011, “Incorporating Source Directionality into Outdoor Sound Propagation Calculations,” *Journal of the Acoustical Society of America*, 130(6), 3608–3622.

VIII. * List of Figures

IX. * List of Tables